0026-895X/08/7305-1413–1423$20.00
MOLECULAR PHARMACOLOGY

Mol Pharmacol 73:1413–1423, 2008

Vol. 73, No. 5
43588/3330549
Printed in U.S.A.

Slc39a14 Gene Encodes ZIP14, A Metal/Bicarbonate Symporter: Similarities to the ZIP8 Transporter

Kuppuswami Girijashanker, Lei He, Manoocher Soleimani, Jodie M. Reed, Hong Li, Zhiwei Liu, Bin Wang, Timothy P. Dalton, and Daniel W. Nebert

Department of Environmental Health and Center for Environmental Genetics (K.G., L.H., J.M.R., Z.L., B.W., T.P.D., D.W.N.) and Department of Internal Medicine, Division of Nephrology and Hypertension (H.L., M.S.), University of Cincinnati Medical Center, Cincinnati, Ohio

Received November 18, 2007; accepted February 12, 2008

ABSTRACT

The mouse and human genomes contain 14 highly conserved *SLC39* genes. Viewed from an evolutionary perspective, *SLC39A14* and *SLC39A8* are the most closely related, each having three noncoding exons 1. However, *SLC39A14* has two exons 4, giving rise to Zrt- and Irt-related protein (ZIP)ZIP14A and ZIP14B alternatively spliced products. C57BL/6J mouse ZIP14A expression is highest in liver, duodenum, kidney, and testis; ZIP14B expression is highest in liver, duodenum, brain, and testis; and ZIP8 is highest in lung, testis, and kidney. We studied ZIP14 stably retroviral-infected mouse fetal fibroblast cultures and transiently transfected Madin-Darby canine kidney (MDCK) polarized epithelial cells. Our findings include: 1) ZIP14-mediated cadmium uptake is proportional to cell toxicity, but manganese is not; 2) ZIP14B has a higher affinity than ZIP14A toward Cd^{2+} (K_m = 0.14 versus 1.1 μM) and Mn^{2+} uptake (K_m = 4.4 versus 18.2 μM); 3) ZIP14A- and ZIP14B-mediated Cd^{2+} uptake is most inhibited by Zn^{2+}, and next by Mn^{2+} and Cu^{2+}; 4) like ZIP8, ZIP14A- and ZIP14B-mediated Cd^{2+} uptake is dependent on extracellular HCO_3^-; 5) like ZIP8, ZIP14 transporters are localized on the apical surface of MDCK-ZIP cells; and 6) like ZIP8, ZIP14 proteins are glycosylated. Tissues such as intestine and liver, located between the environment and the animal, show high levels of ZIP14; given the high affinity for ZIP14, Cd^{2+} is likely to act as a rogue hitchhiker—displacing Zn^{2+} or Mn^{2+} and entering the body to cause unwanted cell damage and disease.

Cadmium is a toxic nonessential divalent cation classified by International Agency for Research on Cancer (Lyon, France) as a "Category I" human lung carcinogen. Acute doses lead to immediate damage in the central nervous system, lung, bone, gastrointestinal tract, liver, placenta, developing embryo, ovary, and testis (Waisberg et al., 2003; Zalups and Ahmad, 2003). Long-term exposure to low Cd^{2+} doses primarily causes renal proximal tubular metabolic acidosis and osteomalacia (renal Fanconi syndrome); Cd^{2+} is eliminated very slowly from the body and thus accumulates (predominantly in kidney, less in liver) as a total body burden with age.

Sources of Cd^{2+} include cigarette smoke, contaminated soil (around metal-smelting operations), and polluted foods such as shellfish. Curiously, tobacco plants take up and concentrate large amounts of Cd^{2+}. Dump sites for toxic waste contain Ni^{2+}-Cd^{2+} batteries; these metals often leach into the groundwater, ultimately entering the human food chain. Cd^{2+} is ranked seventh among the "Top 20 Hazardous Substances Priority List" by the Agency for Toxic Substances and Disease Registry and the U.S. Environmental Protection Agency (Fay and Mumtaz, 1996). People at highest risk for Cd^{2+}-induced lung cancer and chronic nephropathy include cigarette smokers, women having low body-iron stores, persons on a habitual diet rich in high-fiber foods or contaminated shellfish, and malnourished populations (Järup et al., 1998; Järup, 2002, 2003; Waalkes, 2003).

This work was supported in part by National Institutes of Health grants R01-ES10416 (to D.W.N.), R01-DK62809 (to M.S), and P30-ES06096 (to T.P.D., D.W.N.)

K.G. and L.H. contributed equally to this work and are co-first authors.

This work has been presented in part at the 45th Annual Meeting of the Society of Toxicology; 2006 Mar 5–9; San Diego, CA, and the 46th Annual Meeting of the Society of Toxicology; 2007 Mar 25–29; Charlotte, NC.

Article, publication date, and citation information can be found at http://molpharm.aspetjournals.org.

doi:10.1124/mol.107.043588.

ABBREVIATIONS: ZIP, Zrt- and Irt-related protein; TM, transmembrane domain ; HBSS, Hanks' balanced salt solution; MFF, mouse fetal fibroblast; MDCK, Madin-Darby canine kidney; PCR, polymerase chain reaction; bp, base pair(s); HA, hemagglutinin; DIDS, 4,4′-diisothiocyanatostilbene-2,2′-disulfonic acid; PNGase F, peptide *N*-glycosidase F [peptide-N^4-(*N*-acetyl-β-glucosaminyl)asparagine amidase]; SLC, solute carrier; dbEST, database for expressed sequence tags; rvZIP14, vZIP8, rvZIP4, rvLUC, retrovirally infected MFF cells expressing ZIP or firefly luciferase; NBC1, sodium-bicarbonate-1 cotransporter; vMDCK-ZIP14, MDCK-ZIP8, transiently transfected MDCK cells expressing ZIP or firefly luciferase; PBS, phosphate-buffered saline.

For the past 80 years, Cd^{2+} uptake into mammalian cells has been presumed to take place before Cd^{2+}-mediated disease can occur. One possibility for Cd^{2+} influx into mammalian cell cultures is by way of Ca^{2+} channels (Shibuya and Douglas, 1992; Hinkle and Osborne, 1994; Olivi and Bressler, 2000; Bergeron and Jumarie, 2006). SLC11A2 has a preference for Fe^{2+} but also transports Pb^{2+} and Cd^{2+} (Bressler et al., 2004); for this transporter, Cd^{2+} influx is proton-dependent (Bressler et al., 2004). Using SLC11A2 knockdown studies in human intestinal Caco-2 cells (Bannon et al., 2003), proton-dependent Cd^{2+} transport has been demonstrated. Other studies have suggested that SLC11A2 participates in Cd^{2+} transport in gastrointestinal enterocytes (Elisma and Jumarie, 2001; Tallkvist et al., 2001; Park et al., 2002) and renal distal tubular cells (Olivi et al., 2001; Park et al., 2002). Consistent with these studies, Cd^{2+} transport in *Xenopus laevis* oocytes expressing human SLC11A2 shows Michaelis-Menten kinetics with a K_m of 1.04 ± 0.13 μM (Okubo et al., 2003).

Still, no definitive genotype-phenotype association (i.e., a particular gene attributed to Cd^{2+}-induced disease) was reported until 2005. Recent studies have shown such a relationship: allelic differences in the mouse *Slc39a8* gene are responsible for striking variability in risk of Cd^{2+}-induced testicular necrosis among different inbred mouse strains (Dalton et al., 2005), as well as Cd^{2+}-induced acute renal failure (Wang et al., 2007). *Slc39a8* encodes the ZIP8 transporter, which undoubtedly also transports an essential divalent cation. Although Mn^{2+} was shown to be the best inhibitor of ZIP8-mediated Cd^{2+} uptake and has a very low K_m value for ZIP8-mediated uptake (2.2 μM) (He et al., 2006), we believe that zinc (Zn^{2+}) cannot be ruled out as a substrate for ZIP8. Indeed, in studies with *X. laevis* oocytes (Liu et al., 2008), K_m values for Cd^{2+} and Zn^{2+} were recently shown to be ~0.48 and ~0.26 μM, respectively. Cd^{2+} probably displaces Mn^{2+} or Zn^{2+} and operates as a rogue hitchhiker, entering cells via ZIP8 and subsequently contributing to cell death, cancer, and other diseases (He et al., 2006; Wang et al., 2007).

The ZIP8 transporter is a metal/bicarbonate symporter (He et al., 2006). ZIP8 is localized on apical surfaces (He et al., 2006) of several cell types: between the blood and vascular endothelial cells of the testis (Dalton et al., 2005; Wang et al., 2007), and between the glomerular filtrate and proximal tubular epithelial cells of the kidney (Wang et al., 2007). ZIP8 therefore seems to act as a "gatekeeper" for maintaining intracellular Zn^{2+} and perhaps Mn^{2+} homeostasis. On the other hand, however, ZIP8 can serve as a means for bringing unwanted environmental Cd^{2+} into the organism. In terms of evolution, the closest neighbor to ZIP8 is ZIP14, encoded by the *SLC39A14* gene. The present study provides the complete characterization of this gene and its ZIP14 mRNAs and proteins and for the first time demonstrates the significance of ZIP14 in Cd^{2+}-mediated cell damage.

Materials and Methods

Bioinformatics Tools. Protein sequences and their respective ZIP domains were obtained from the NCBI website (http://www.ncbi.nlm.nih.gov). ClustalW (http://www.ebi.ac.uk/clustalw/index.html) was used to construct a multiple alignment and phylogenetic tree of human and mouse ZIP proteins. Only the ZIP domain sequences of each protein were "joined" to each other and used to construct this tree. To assess the topology and transmembrane (TM) domain sequences of ZIP proteins, each protein sequence was submitted to the online program MINNOU (membrane protein identification, without explicit use of hydropathy profiles and alignments) at http://minnou.cchmc.org/ to detect the putative TM regions (Cao et al., 2006). Only the TM domain sequences were used in generating an artificial sequence for each protein. Percentage identity was then assessed, based on only the pair-wise alignment of these artificial sequences.

Chemicals. All divalent cations, plus Fe^{3+}, were purchased as chloride salts from Thermo Fisher Scientific (Waltham, MA). The remainder of the chemicals was purchased from Sigma (St. Louis, MO). $^{109}CdCl_2$ [710 mCi/mg (1 mCi = 37 mBq) in 0.1 M HCl] was purchased from GE Healthcare (Chalfont St. Giles, Buckinghamshire, UK), $^{54}MnCl_2$ [7734 mCi/mg in 0.5 M HCl] was from Perkin-Elmer Life and Analytical Sciences (Waltham, MA), and $^{65}ZnCl2$ [140 mCi/mg in 0.1 M HCl] from the National Laboratory of Oak Ridge (Oak Ridge, TN). Uptake medium was a modified version of Hanks' balanced salt solution (HBSS), as detailed (He et al., 2006).

Cell Cultures. Mouse fetal fibroblast (MFF) cells (Dalton et al., 2005) or Madin-Darby canine kidney (MDCK) cells (American Type Culture Collection; Manassas, VA) were cultured at 37°C in 5% CO_2 in Dulbecco's modified Eagle's medium (Invitrogen, Carlsbad, CA) plus 10% fetal bovine serum (Hyclone, Logan, UT). All details of the culture medium have been described previously (Dalton et al., 2005; He et al., 2006).

Quantitative Polymerase Chain Reaction Analysis. Total RNA was isolated from six tissues of untreated C57BL/6J mice. Total RNA (2.5 μg) was used as a template for reverse transcription in 20 μl and then primed with oligo(dT) using the SuperScript III first-strand kit (Invitrogen), according to the manufacturer's recommendations. The plasmids pBlueScript-ZIP14A-HA, pBlueScript-ZIP14B-HA, and pXFRM-ZIP8-HA were used to establish calibration curves, which were then used to quantify the ZIP14A, ZIP14B, and ZIP8 mRNA copy numbers, respectively, in each tissue. The absolute copy number of each plasmid can be calculated as the "copy number = mass (in grams) × (6.023×10^{23}) / molecular weight. To prepare the calibration curve, we first did a serial dilution (10^{-1}, 10^{-2}, 10^{-3}, 10^{-4}, 10^{-5}, 10^{-6}, 10^{-7}, 10^{-8} μg/PCR reaction) for each plasmid; each point was analyzed in duplicate using the same PCR settings as we had used in analyzing the experimental samples. The average ΔC_t value at each point was then used to plot the linear calibration curves [$\log_{10}$ (mass) versus ΔC_t]. Finally, the linear regression equation and correlation value r (to reflect goodness of fit) were determined. Each ΔC_t value from an experimental sample could be converted to the absolute copy number of transcripts, based on this equation. PCR primers for mRNA were as follows: for Z14A: forward, 5′-TTCCTCAGTGTCTCACTGATTAA-3′; reverse, 5′-GGAAAAGGGCGTTAGAGAGC-3′ (PCR product is 142 bp); for Z14B: : forward, 5′-CATTGAAGTATGGGGGTACGGT-3′; reverse, 5′-ATGAAGTAGAGCAGGAGCCTCT-3′ (PCR product is 122 bp). PCR primers for the ZIP8 mRNA were: forward, 5′-GCAACAATTTTGCTCCCAAT-3′; reverse, Zip8-R 5′-TCCCTATGGAGATGTTTCTGTG-3′ (PCR product is 291 bp).

The range of calibration curves was linear from 10^3 to 10^7 μg of plasmid (r = 0.999 for ZIP14A, 0.998 for ZIPB and 0.995 for ZIP8). Quantitative reverse transcription-PCR reactions were performed in triplicate in a mixture containing 1× Power SYBR Green PCR Master Mix (Bio-Rad Laboratories, Hercules, CA) on a DNA engine2 real-time PCR system (MJ Research, Watertown, MA). Using 1 μl from step 1, the 20-μl reaction (0.125 μg of total RNA) was heated to 95°C for 10 min and immediately cycled 40 times through a denaturing step at 95°C for 15 s, an annealing at 58°C for 30 s, and an elongation step at 72°C for 45 s. Melting curve analyses were performed after PCR amplification to ensure that a single product with the expected melting curve characteristics was obtained—as preliminarily determined during primer tests.

Cloning of the ZIP14 cDNAs and Delivery into MFF or MDCK Tet-off Cells. Oligo-dT-primed reverse transcription was carried out with C57BL/6J mouse liver total RNA. Primers for amplification began at the ZIP14 cDNAs' start codon and ended at the stop codon; a consensus Kozak sequence at the start site was included for efficient expression. For ZIP14A and ZIP14B, restriction sites were added at the 5′ (BamHI) and 3′ (ApaI) ends of the coding sequence for cloning into the pRevTRE vector (Invitrogen). Restriction sites for ZIP8 and ZIP4, procedures for inserting a hemagglutinin (HA) tag in-frame at the C terminus and infection of MFF cell cultures with a retrovirus encoding the Tet-off receptor (Bergwitz et al., 2000) have been detailed previously (Dalton et al., 2005; He et al., 2006). These procedures resulted in stable rvLUC (as the ZIP-absent luciferase control), rvZIP14Aha, rvZIP14Bha, rvZIP8ha, and rvZIP4ha MFF cell cultures. Transiently transfected MDCK cells are denoted by "MDCK-" at the beginning.

Determination of Cd^{2+} and Mn^{2+} Uptake. The procedures for measuring radiolabeled Cd^{2+} and Mn^{2+} uptake have been detailed previously (Dalton et al., 2005; He et al., 2006).

Cell Survival after Cd^{2+} or Mn^{2+} Treatment. The methods for measuring cell viability, using the 3-(4,5-dimethlythiazol-2-yl)-2,5-diphenyl tetra[*b*]zolium bromide assay, have been described previously (Dalton et al., 2005; He et al., 2006).

Inhibition of Cd^{2+} Uptake by Other Metal Ions. The procedures for measuring competitive inhibition of Cd^{2+} uptake by divalent and trivalent cations have been detailed previously (Dalton et al., 2005; He et al., 2006).

***K_m* Determination.** Cells grown in HBSS were treated with $^{109}CdCl_2$, $^{54}MnCl_2$ or $^{65}ZnCl_2$ at six different concentrations, as detailed previously (He et al., 2006). The uptake data at the different concentrations were entered into the Enzyme Kinetics Module, an add-on software program of SigmaPlot (Systat Software, Inc., San Jose, CA).

Dependence on pH, Other Ions, Energy, and Temperature. The procedures for measuring these parameters have been detailed previously (He et al., 2006).

Dependence on HCO_3^- for Cd^{2+} Uptake. The procedures for measuring HCO_3^- dependence, including inhibition by 4,4′-diisothiocyanatostilbene-2,2′-disulfonic acid (DIDS), a well known competitive inhibitor of HCO_3^- transporters, have been described previously (He et al., 2006).

Z-Stack Confocal Microscopy for Distinguishing between Apical and Basolateral Location. MDCK cells were seeded onto cover slips in a 24-well plate. Next day, when the cells reached 90% confluence, the cells were transfected according to the manufacturer's protocol for Lipofectamine 2000 (Invitrogen) with the combination of the following plasmids: pRevTet-Off and pRevTRE-ZIP14Aha or pRevTet-Off and pRevTRE-ZIP14Bha. Some wells were transfected with the plasmid encoding green fluorescent protein-NBC1, known to localize to the basolateral surface. The rest of the protocol for carrying out Z-stack confocal microscopy in transiently transfected confluent monolayers of MDCK polarized epithelial cells has been detailed (Li et al., 2005; He et al., 2006). In general, 0.4- to 1.0-μm fixed interval cuts were carried out, and 20 to 30 images were generated as a gallery. The images (*x*-*y* projections) and corresponding *z*-lines (*x*-*z* or *y*-*z* projections) and tangential cuts were subsequently obtained.

Western Immunoblot Analysis of ZIP14 Protein Glycosylation. Peptide *N*-glycosidase F (PNGase F; New England Biolabs, Ipswich, MA) is an amidase that cleaves between the innermost *N*-acetylglucosamine and asparagine residues of high mannose, hybrid, and complex oligosaccharides from *N*-linked glycoproteins. The procedures for performing Western immunoblots, with and without PNGase F, to assess ZIP14 glycosylation, have been described previously (He et al., 2006).

Statistical Analysis. Statistical significance between groups was determined by analysis of variance between each group and/or Student's *t* test. All assays were performed in duplicate or triplicate and repeated at least twice. Statistical analyses were performed with the use of SAS statistical software (SAS Institute Inc., Cary, NC). The determinations of K_m and V_{max} values for ZIP-mediated metal uptake, metal competition studies, and EC_{50} values (concentrations at which cell survival was 50% of maximum), were determined using Sigma Plot (SPSS Inc., Chicago, IL).

Results

Evolutionary Analysis and Bioinformatics. The solute-carrier (SLC) gene superfamily comprises 46 families and 360 putatively functional transporter genes in the human genome (Hediger et al., 2004). No homology is shared among the 46 families; however, at least 20–25% amino acid sequence identity (i.e., a specific "signature sequence") is shared by members within any *SLC* family. Figure 1A shows the phylogenetic tree of the *SLC39* family. Mouse and human have 14 *SLC39* genes; each of the 14 genes in mouse has an ortholog in human that is highly conserved. It can be seen from the dendrogram that ZIP14 and ZIP8 are most closely related to one another and distantly related to all of the other 12 members of this family.

Further analysis of the mouse *Slc39a14* gene structure (Fig. 1B) revealed that this gene is highly similar to the mouse *Slc39a8* in that they both have nine exons, as well as three noncoding exons 1 that denote alternative transcription start sites. The translation open reading frame begins in

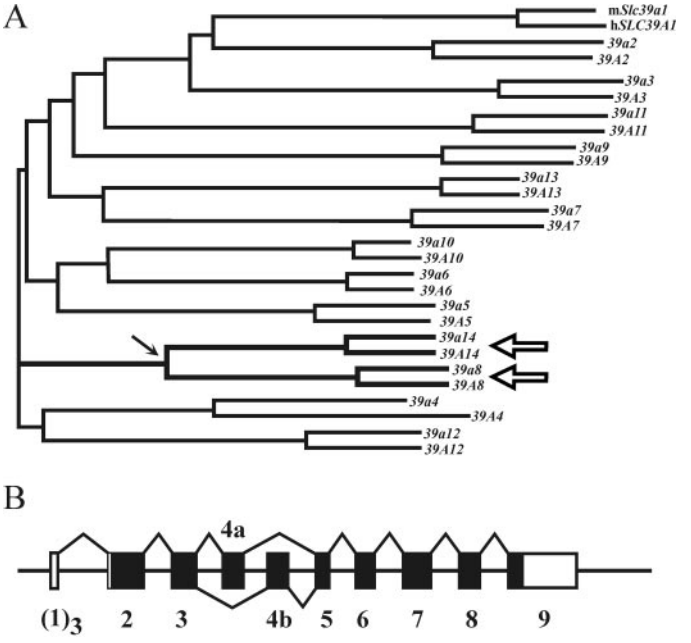

Fig. 1. A, nearest-neighbor joining (NNJ)-generated phylogenetic tree of the 14 mouse and 14 human ZIP domains of the *SLC39* gene-encoded proteins. These amino acid fragments were ligated, aligned, and then compared to determine percentage identity. In terms of evolution, the mouse *Slc39a14* and *Slc39a8* and human *SLC39A14* and *SLC39A8* members (large open arrows) are most closely related and diverged from one another (small arrow) sometime after the land animal-sea animal split ~425 million years ago (see *Discussion*). B, structure of the mouse *Slc39a14* genomic gene (introns not drawn to scale) illustrating the alternatively spliced exons 4, which encode the ZIP14A and ZIP14B proteins, respectively. Similar to *Slc39a8* (Dalton et al., 2005), the *Slc39a14* gene also has three alternatively spliced nontranslated exons 1. Of the nine exons (*rectangles*), the coding region is *closed*, and the 5′ and 3′ UTRs are open. The human *SLC39A14* gene has the same highly conserved structure as the mouse gene, except that exons 1b and 1c have not been identified (see Table 1 and text).

exon 2 and ends in exon 9. Between mouse and human, each internal exon has very similar, if not identical, lengths, and the exon-intron junctions are highly conserved (Table 1). Between mouse and human, *SLC39A14* exons 3, 4, 6, 7, and 8 have identical bp numbers, whereas human *SLC39A14* exon 5 is 3 bp longer. Between mouse and human, *SLC39A8* exons 3, 4, 5, 7, and 8 have an identical number of base pairs, whereas mouse *Slc39a8* exon 6 is 6 bp longer. The mouse and human ZIP14 transporter proteins contain 489 and 492 amino acids, respectively.

Note that, so far, none of the mouse or human genome databases has thoroughly cataloged the alternatively spliced exons 1 of mouse *Slc39a14* or mouse or human *SLC39A8*; this is probably because of the shortcomings of present-day "gene-finder" software programs. By comparing the dbEST with genome databases, we were able to find mRNAs that included the exons 1 of mouse *Slc39a14* and of mouse and human *SLC39A8*. We discovered no evidence, however, of alternatively spliced exons 1 for the human *SLC39A14* gene (Table 1). Either these exons 1 exist but have not yet been captured in the dbEST or these exons 1b and 1c became no longer useful in the human ancestral branch and diverged into sequences that are no longer detectable.

During the ZIP14 cDNA cloning process and while studying the dbEST, we also discovered exons 4A and 4B; when alternatively spliced, this resulted in ZIP14A, ZIP14B, and ZIP14AB cDNAs (Fig. 1B). The ZIP14AB transcript has a disrupted open reading frame and would encode a truncated protein with only 157 amino acids; therefore, we did not study ZIP14AB further. Mouse *Slc39a14* exons 4A and 4B are both 170 bp long (Table 1) and share 67% nucleotide identity (Fig. 2). Transcripts of ZIP14A and ZIP14B encode two different proteins, both having 489 amino acids but molecular masses of 53,754 and 53,962 Da, respectively. These two proteins differ only in the 57-amino acid region encoded by the alternative exons 4; of the 57 amino acids, 37 are identical and 20 are different. This segment includes almost all of TM1, the intracellular loop between TM1 and TM2, and almost all of TM2 (Fig. 2). Yet differences in exon 4 seem not to change the topology of the two transporter proteins. Percentage identity in the ZIP domain sequences, between mouse and human, is 92% for ZIP14 and 96% for ZIP8. Mouse ZIP14A and ZIP14B are both 73% identical to ZIP8 in the ZIP domain (Fig. 2). In contrast, for example, mouse ZIP14A and ZIP14B share 41% identity with mouse ZIP4 and 15% identity with mouse ZIP1.

Tissue Distribution of ZIP14 versus ZIP8 mRNA. Q-PCR analysis of C57BL/6J mice revealed ZIP14A mRNA levels that were highest in liver > duodenum > kidney > testis > brain = lung and ZIP14B mRNA levels highest in liver = duodenum > brain = testis > kidney = lung (Fig. 3). In contrast, ZIP8 mRNA levels were highest in lung = testis > kidney ≫ liver > brain > duodenum. The ZIP14A/ZIP14B ratio is maximal (7.8-fold) in liver, next highest (~4-fold) in kidney and duodenum, and lowest (0.7-fold) in brain. Total ZIP14 transcripts are 39- and 18-fold greater than ZIP8 transcripts in duodenum and liver, respectively, whereas ZIP8 transcripts are 12- and 5-fold greater than total ZIP14 transcripts in lung and testis, respectively.

Effect of Metal Uptake on Cell Survival. Note that rvZIP14A cells transported both Cd^{2+} and Mn^{2+} substantially better than rvZIP14B cells (Fig. 4A). In control rvLUC cells, Cd^{2+} or Mn^{2+} uptake was very low during the 60-min experiment. Consistent with the Fig. 4A data, the ZIP14A transporter (Table 2) exhibited a 3- to 5-fold greater V_{max} for Cd^{2+} and Mn^{2+} uptake than the ZIP14B transporter. The V_{max} for Cd^{2+} uptake by ZIP8 was not statistically different from that by ZIP14A and more than 3-fold higher than that by ZIP14B (Table 2). On the other hand, the V_{max} for Mn^{2+} uptake by ZIP8 was 15 times less than that by ZIP14A and 4.5 times less than that by ZIP14B. Differences in maximum rates of transport (V_{max}) could very easily reflect differences in expression of the constructs or differences in trafficking of the transporter to the cell surface. In contrast, neither of these cellular processes influenced the K_m value.

In terms of K_m values, ZIP14B showed a ~8-fold greater

TABLE 1

Comparison of the mouse and human *SLC39A14* and *SLC39A8* gene structures

All sequences are based on NCBI m37 mouse assembly (Apr 2007; strain C57BL/6J) and NCBI 36 assembly of the human genome (Nov 2005). From the 5′-most (exon 1c) start site to the 3′-most nucleotide of exon 9, the four genes from left to right span 92,502, 57,942 [?], 64,860, and 88,148 bp, respectively. For mouse *Slc39a14*, the genomic 5′ to 3′ sequence is exon 1c, intron 1c, exon 1b, intron 1b, exon 1a, intron 1a, exon 2, intron 2, exon 3, intron 3, exon 4a, intron 4a, exon 4b, intron 4b, exon 5, intron 5, … … exon 9.

Number	Mouse *Slc39a14*		Human *SCL39A14*		Mouse *Slc39a8*		Human *SLC39A8*	
	Exon	Intron	Exon	Intron	Exon	Intron	Exon	Intron
	bp		*bp*		*bp*		*bp*	
1c	139	32,340	[?]	[?]	256	1486	184	801
1b	110	29,383	[?]	[?]	146	632	139	429
1a	131	15,130	104	37,287	37	156	26	159
2	279	2037	285	3329	451	22,325	748	28,613
3	187	604	187	1449	163	6725	163	8062
4(a)	170	4688	170	4664	170	1409	170	2324
4(b)	170	2625	170	2573				
5	120	584	123	866	123	465	123	507
6	189	117	189	115	171	25,955	165	36,237
7	208	923	208	1370	208	197	208	197
8	185	1837	185	1716	185	2018	185	4296
9	516		3122		1582		1527	
Total[a]	1993[a]	90,268	[4573 bp]	[53,369 bp]	3309	61,368 bp	3473	84,510
	1964				3199		3428	
	1985				3090		3315	

[?], not detected in the human genome.

[a] The three total lengths of exons denote the mRNA transcripts using exons 1c, 1b, or 1a, respectively (which are found in the dbEST database).

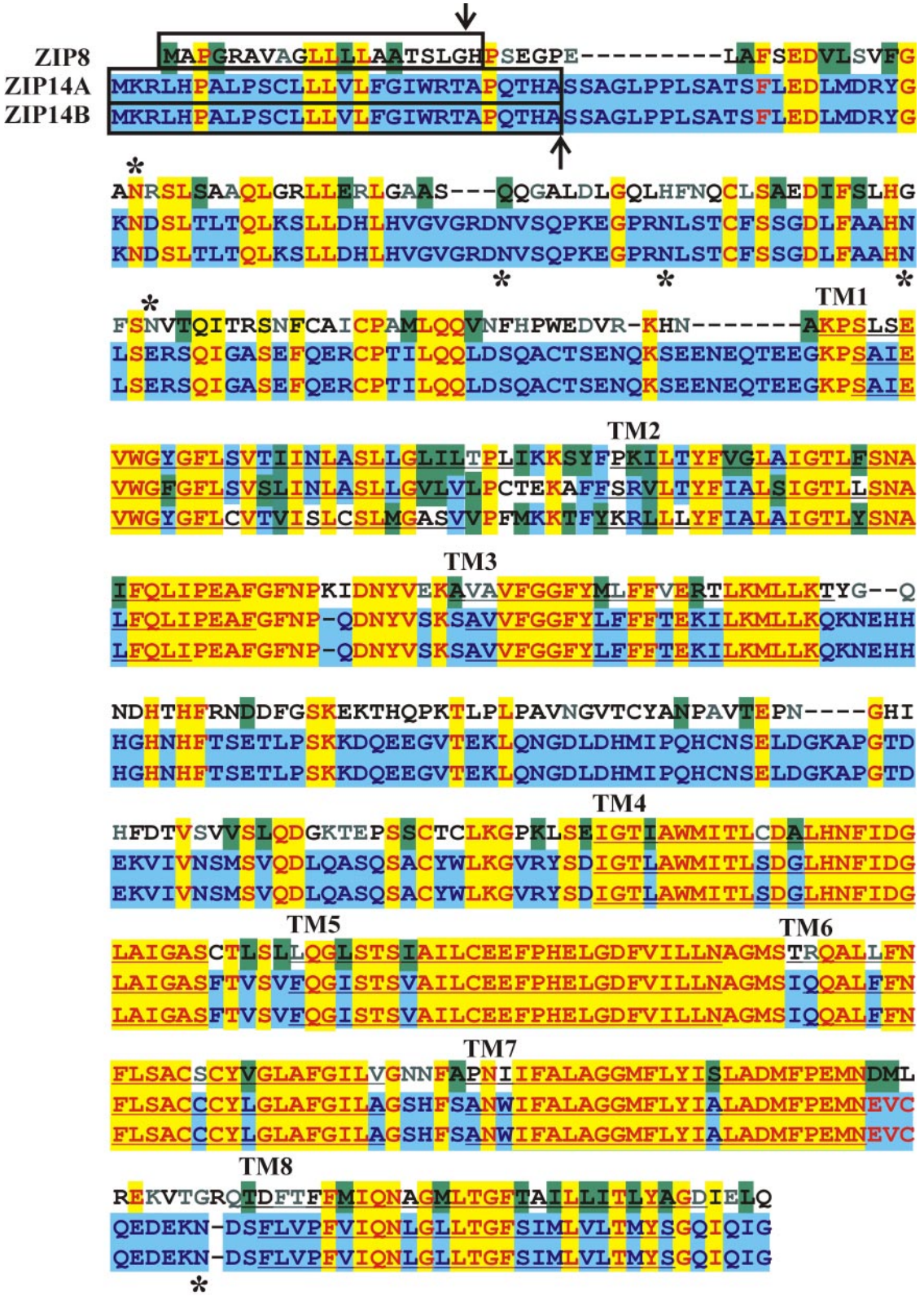

Fig. 2. Alignment of mouse ZIP8 (top), ZIP14A (middle), and ZIP14B (bottom) proteins. The only differences between ZIP14A and ZIP14B occur in the alternatively spliced exon 4, which results in 57 amino acids (from Val151 through Glu207). ZIP8 is 73% identical to ZIP14A, and ZIP8 is 73% identical to ZIP14B (in the ZIP domain only). ZIP14A is 67% identical to ZIP14B in exon 4. Boxes show the N terminus putative membrane localization signal. Arrows denote possible cleavage sites to render the mature membrane-bound proteins. Asterisks indicate potential glycosylation sites. The eight putative transmembrane (TM) regions are underlined and denoted as "TM1" through "TM8" (labeled in each case at the left end). The precise amino acid at which a TM domain begins or ends reflects the software program and could be off by a residue or two; there are no experimental data to support this. The mouse and human ZIP14 transporter proteins comprise 489 and 492 amino acids, respectively. In contrast, the mouse and human ZIP8 proteins contain 462 and 461 amino acids, respectively. Black-on-white denotes nonsimilar residues; blue-on-cyan denotes a consensus residue derived from a block of similar residues at a given position; black-on-green denotes a consensus residue derived from the occurrence of >50% of a single residue at a given position; red-on-yellow denotes a consensus residue derived from a completely conserved residue at a given position; green-on-white denotes a residue weakly similar to a consensus residue at a given position.

affinity for Cd^{2+} and ~4-fold greater affinity for Mn^{2+} than ZIP14A (Table 2). ZIP8 showed almost 2-fold greater affinity for Cd^{2+} than ZIP14A and 4 times less affinity than ZIP14B. ZIP8 showed 8-fold greater affinity for Mn^{2+} than ZIP14A and 2-fold greater affinity for Mn^{2+} than ZIP14B.

The survival curves for cells exposed to Cd^{2+} were not significantly different among rvZIP14A, rvZIP14B, and rvZIP8 cells (Fig. 4B). In contrast, rvLUC control cells and rvZIP4 cells displayed at least 20-fold greater cell survival—because of their relative inability to take up Cd^{2+} (He et al., 2006). On the other hand, increasing Mn^{2+} concentrations showed no more than 2-fold differences in cell survival for rvZIP8, rvZIP14A, and rvZIP14B, compared with that for rvZIP4 or rvLUC cells (Fig. 4B), even though the difference in Mn^{2+} uptake by ZIP14A or ZIP14B was very substantial, compared with that by control cells (Fig. 4A).

Metal-Mediated Competitive Inhibition of Cd^{2+} Uptake. Fig. 5 shows that Zn^{2+} was by far the best inhibitor of

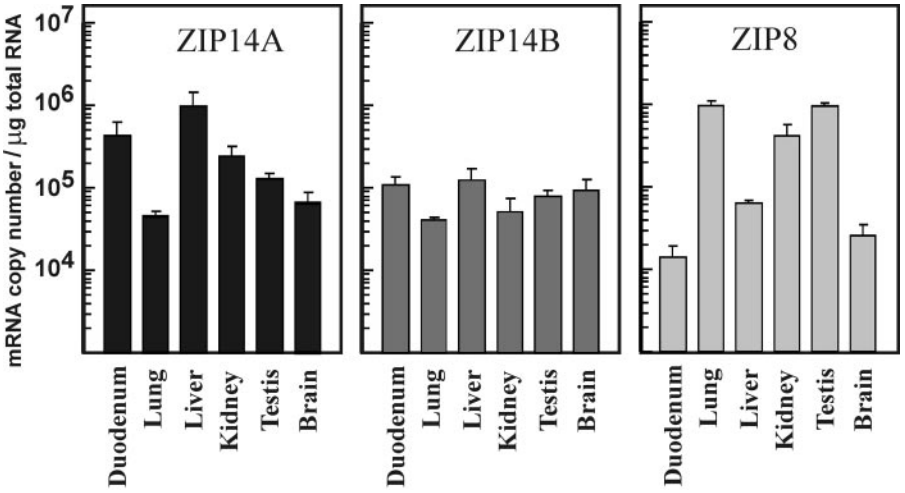

Fig. 3. Comparison of ZIP14A, ZIP14B, and ZIP8 mRNA levels in six tissues of the untreated C57BL/6J mouse. Values are expressed as means ± S.E. (n = 3 mice).

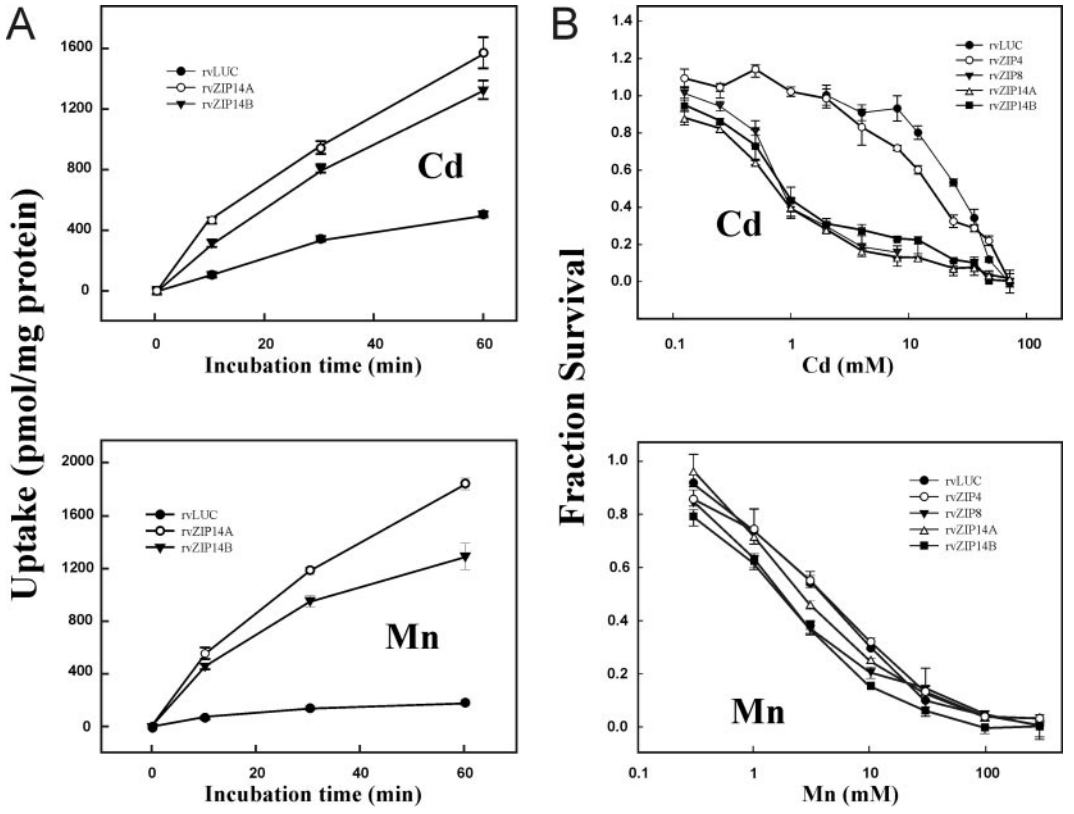

Fig. 4. A, comparison of Cd^{2+} versus Mn^{2+} uptake kinetics by retroviral (rv) stably transfected MFF cultures in HBSS. Cells were exposed to 0.25 μM Cd^{2+} (spiked with $^{109}CdCl_2$) or 0.25 μM Mn^{2+} (spiked with $^{54}MnCl_2$) for 60 min at 37°C. rvLUC, control cells having no ZIP protein. B, semi-log plot of cell survival as a function of increasing doses of Cd^{2+} or Mn^{2+}, in four rvZIP cell lines versus rvLUC control cells. Cultures were exposed to the indicated concentrations of Cd^{2+} or Mn^{2+} for 32 h at 37°C in Dulbecco's modified Eagle's medium containing 10% fetal bovine serum. After Cd^{2+} exposure, the rvZIP8, rvZIP14A, and rvZIP14B lines are significantly different ($P < 0.001$) from the rvZIP4 and rvLUC lines at all Cd^{2+} concentrations between 0.6 and 30 mM. After Mn^{2+} exposure, the rvZIP8, rvZIP14A, and rvZIP14B lines are significantly different ($P < 0.05$) from the rvZIP4 and rvLUC lines at all Cd^{2+} concentrations between 0.3 and 10 mM. Cell survival was monitored using the 3-(4,5-dimethylthiazol-2-yl)-2,5-diphenyl tetrasodium bromide assay. Values are expressed as means ± S.E. (n = 3 wells; two experiments done in different weeks).

TABLE 2

Comparison of transport kinetics of ZIP14A-, ZIP14B-, and ZIP8-mediated Cd^{2+} versus Mn^{2+} uptake

Cells were grown in Dulbecco's modified Eagle's medium until 60 min before the experiment, at which time the medium was changed to HBSS. All measurements were made under conditions of the initial linear-uptake rate. Values are expressed as means ± S.E.

	Cadmium			Manganese		
	ZIP14A	ZIP14B	ZIP8[a]	ZIP14A	ZIP14B	ZIP8[a]
V_{max} (pmol/min/mg protein)	113 ± 12	25 ± 3	92.1 ± 10	1140 ± 100	330 ± 29	73.8 ± 6
K_m (mM)	1.1 ± 0.02	0.14 ± 0.02	0.62 ± 0.07	18.2 ± 2	4.4 ± 0.5	2.2 ± 0.3

[a] ZIP8 uptake kinetics was reported previously (He et al., 2006).

Cd^{2+} uptake by both rvZIP14A and rvZIP14B cells. Tied for second-best inhibitor were Mn^{2+} and Cu^{2+}. No significant inhibition of Cd^{2+} uptake—by either rvZIP14A or rvZIP14B cells—was seen with Cs^{2+}, Fe^{2+}, or Fe^{3+} ions (Fig. 5).

Other Parameters Affecting ZIP14-Mediated Cd^{2+} Uptake. Cd^{2+} uptake by rvZIP14A or rvZIP14B cells was maximal at 37°C and maximal when (extracellular) pH of the transport medium was 7.5 (data not shown), demonstrating that ZIP14 transporters are not proton-coupled. ZIP14A- and ZIP14B-mediated Cd^{2+} transport was strongly inhibited by cyanide, indicating a dependence on an energy source, such as ATP. Cd^{2+} influx was not affected by any level of Cl^-, Na^+, or K^+ ions added (data not shown), suggesting that none of these ions is coupled to Cd^{2+} transport. These findings are identical to those found with rvZIP8 cells (He et al., 2006).

Dependence of ZIP14-Mediated Cd^{2+} Uptake on HCO_3^- Ion. We found that Cd^{2+} uptake by rvZIP14A or rvZIP14B cells was dependent on extracellular HCO_3^- concentrations, compared with control rvLUC cells (Fig. 6A). Significantly less Cd^{2+} uptake was seen at 0 and 1 mM HCO_3^- than at ≥2 mM. By 4 mM HCO_3^-, Cd^{2+} influx had clearly reached its maximum. The 0 mM HCO_3^- in rvZIP14 cells in HBSS (Fig. 6A) is actually not free of HCO_3^-, because there is exogenous HCO_3^- present from dissolved CO_2 in the air, as well as the CO_2/HCO_3^- derived from cellular metabolism. From the Henderson-Hasselbach equation of this buffer system, $pH = pK + \log([HCO_3^-]/0.03 \times pCO_2)$, one can calculate that putatively "HCO_3^--free" medium at 37°C and pH 7.5 actually contains 171 μM HCO_3^-; this is likely the reason why, at 0 mM HCO_3^- HBSS, we are still able to observe substantial amounts of both ZIP14A- and ZIP14B-mediated Cd^{2+} transport, which are much greater than that seen in rvLUC cells (Fig. 6A).

DIDS is a well known inhibitor of HCO_3^--dependent transporters (Cabantchik and Greger, 1992). To further confirm the dependence of Cd^{2+} uptake on HCO_3^-, we added DIDS to 171 μM HCO_3^--containing HBSS medium before adding Cd^{2+} (Fig. 6B). In the absence of DIDS (far left), Cd^{2+} uptake by rvZIP14A and rvZIP14B was ~180 and ~155 pmol/min/mg protein, respectively (after subtracting Cd^{2+} uptake by rvLUC cells). At the very low levels of 0.125 and 0.25 mM, DIDS inhibited Cd^{2+} uptake in rvZIP14 cells by ~28 and ~44%, respectively. On the other hand, at 1.0 mM DIDS—a concentration regularly used to inhibit 4 mM HCO_3^- uptake—DIDS inhibited Cd^{2+} uptake close to 100% in both rvZIP14A and rvZIP14B cells.

Membrane Localization and Characterization of ZIP14 Transporters. Both ZIP14A and ZIP14B proteins were shown to be localized exclusively to the apical surface of MDCK polarized epithelial cell monolayers; this can best be seen in the apical plane of the *x-y* projections and the *z-y* planes traversing from basal to apical, as well as the tangential cut (Fig. 7, right column and merged middle column). An apical-surface control, lectin (red), and a basolateral-surface control, NBC1 (green), were included in these confocal studies.

Figure 8 illustrates our study with PNGase F. We used HA-tagged proteins because so far we lack an efficient anti-ZIP antibody for Western blots. Glycosylated ZIP14A proteins (third lane) appear as 60- and 70-kDa faint bands; after PNGase F treatment, the native ZIP14A protein is close to its calculated 53,754-Da size (fourth lane). Glycosylated ZIP14B

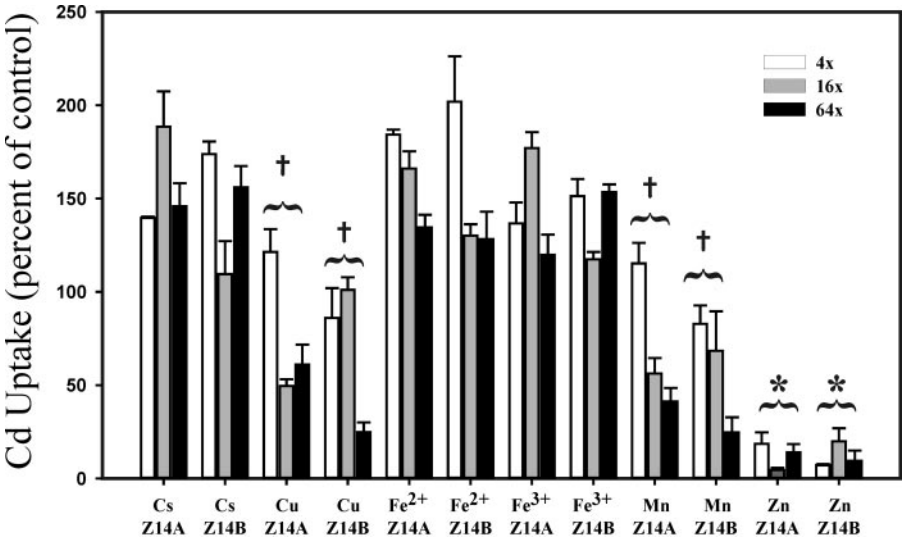

Fig. 5. Metal cation competition for Cd^{2+} uptake in rvZIP14A (Z14A) versus rvZIP14B (Z14B) cells. $^{109}CdCl_2$ was added to make a final Cd^{2+} concentration of 0.25 μM; the competing metal cations (as chloride salts) at concentrations of 0, 1, 4, or 16 μM were added at the same time as Cd^{2+}, and the cells were incubated at 37°C for 20 min, after which Cd^{2+} accumulation was determined. Zn^{2+} was most inhibitory (*, $P = 0.0007$), with Mn^{2+} and Cu^{2+} as second most inhibitory (†, $P < 0.01$). No significant inhibition was seen with Cs^{2+}, Fe^{2+}, or Fe^{3+} ($P > 0.05$). Two-tailed P values were calculated using Student's t test with 4 degrees of freedom.

proteins (fifth lane) appear as a light doublet at ~68 to 72 kDa; after PNGase F treatment, native ZIP14B shows up as two bands, the smaller one close to its calculated 53,962-Da size (sixth lane). A positive control, glycosylated ZIP4 proteins (seventh lane), appear as faint bands in the 80- to 90-kDa range; after PNGase F treatment, the native ZIP4 is close to its calculated 68.4-kDa size (last lane at right).

Discussion

Evolutionary Analysis. The mouse *Slc39a14* and *Slc39a8* genes are far more closely related to one another than to any of the other 12 family members (Fig. 1A). Although both genes have nine exons and three alternative exons 1, *Slc39a14* differs from *Slc39a8* in that it has two exons 4 (Fig. 1B). Excluding additional splice sites in the 3′ untranslated region, this means at least six *Slc39a14* transcripts are possible, if one considers

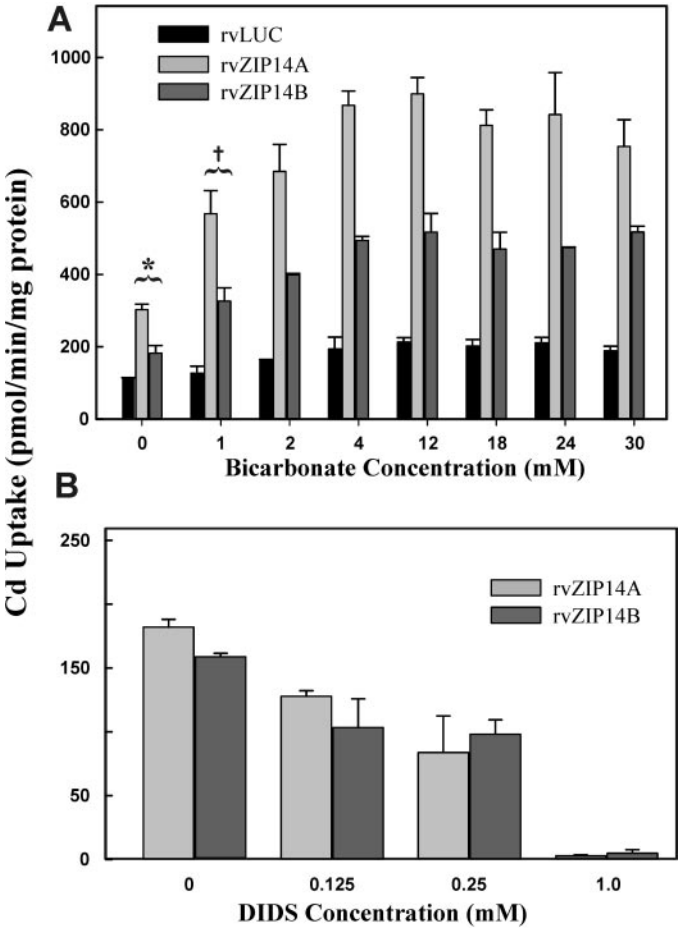

Fig. 6. Dependence of Cd^{2+} uptake on HCO_3^- in the medium. A, Cd^{2+} uptake over a range from 0 to 30 mM HCO_3^- levels in HBSS. The black bars denote Cd^{2+} uptake in rvLUC control cells. At 0 mM HCO_3^- (*, $P < 0.01$) and at 1 mM HCO_3^- (†, $P < 0.05$), Cd^{2+} uptake by both rvZIP14A and rvZIP14B cells was significantly different from that seen at HCO_3^- concentration between 2 and 30 mM. B, Cd^{2+} uptake as a function of increasing DIDS concentrations. Cd^{2+} uptake by rvLUC cells was subtracted from that by the rvZIP14A or rvZIP14B cells. The transport medium contains nominal HCO_3^- concentrations (171 μM). The DIDS solution was prepared fresh in dimethyl sulfoxide and added to the uptake medium 30 min before addition of the Cd^{2+}. In A and B, cells were incubated with 0.25 μM Cd^{2+}, spiked with $^{109}CdCl_2$, for 20 min at 37°C. At all HCO_3^- concentrations and all DIDS concentrations, the pH was maintained at ~7.4, and the balance of anions and cations was carefully controlled for, as detailed in He et al. (2006).

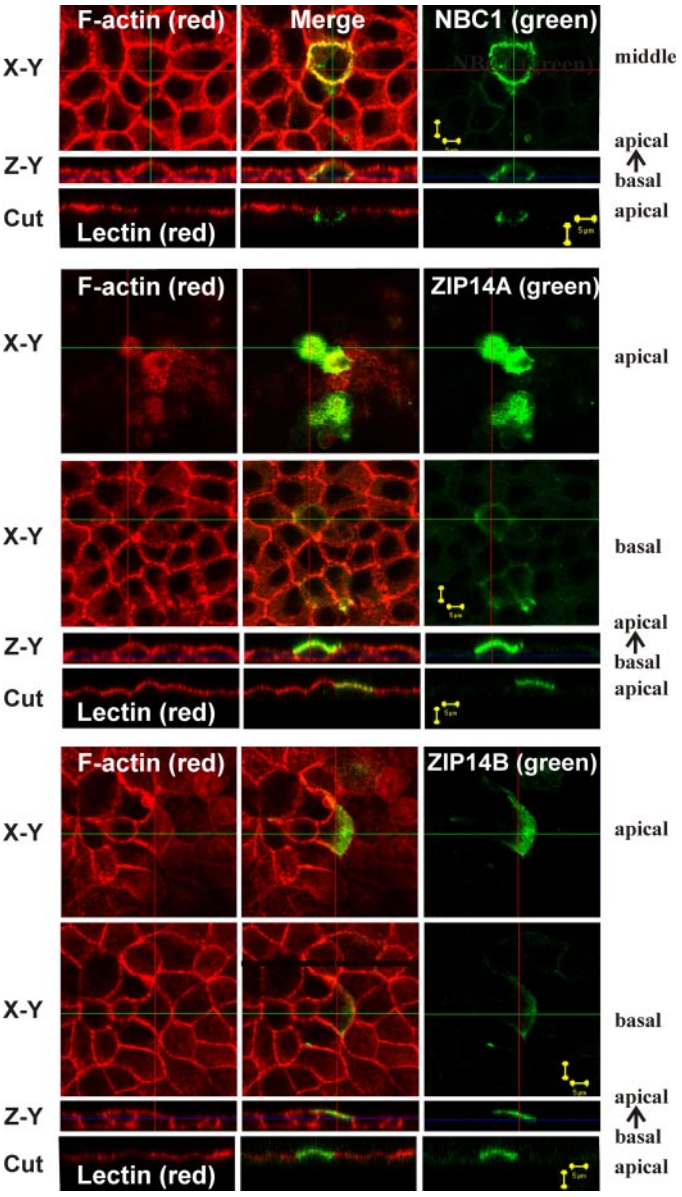

Fig. 7. Z-stack confocal microscopy of MDCK-cell monolayers. Green fluorescent protein-NBC1 expression (top three rows); ZIP14Aha expression (next four rows); ZIP14Bha expression (bottom four rows). Two days after transfection, the confluent cells were incubated in Chelex 100 medium for 1 h, fixed with 3% formaldehyde for 20 min, and then permeabilized with 0.1% Triton X-100 for 4 min and blocked with 10% fetal bovine serum-containing PBS medium for 1 h. All of this was done at room temperature. The α-HA (Bethyl Laboratories, Montgomery, TX), at 1:500 dilution, was incubated at 4°C overnight with cells in 1% bovine serum albumin containing PBS. The next day, the primary antibody solution was removed and the cells were washed three times with PBS for 5 min each time. The secondary antibody Alexa 488-α-rabbit (causing green fluorescence) (Invitrogen) was incubated with the cells at room temperature for 1 h. Cell monolayers were then costained with either a membrane marker (F-actin) phalloidin-tetramethylrhodamine (Invitrogen) or specifically an apical membrane marker peanut agglutinin lectin (Invitrogen) at 1/250 dilution for 20 min at room temperature and then mounted for confocal analysis. The red color (F-actin or lectin) in the left column of panels, plus the green color (NBC1, ZIP14A, ZIP14B) in the right column of panels, are merged together in the middle column of panels. The *x-y* plane for NBC1 expression (top) was taken through the middle, whereas the *x-y* projections for ZIP14A (middle) and ZIP14B (bottom) were taken both through the apical and basal surfaces of the MDCK cells, as labeled. The *Z-Y* plane is at a right angle to the *x-y* plane and illustrates the basal→apical orientation of the polarized epithelial cells. The "Cut" refers to a tangential plane.

all combinations of alternative splicing in exons 1 plus exons 4. These different splice variants might dictate temporal, tissue, or cell-type specificity. This alternative exon splicing pattern of the mouse *Slc39a14* gene was recently reported (Liuzzi et al., 2005) but wrongly attributed to exon 6. From an evolutionary standpoint, these data indicate that, after the vertebrate *SLC39A14* and *SLC39A8* genes diverged, an exon 4 duplication event occurred in the *SLC39A14* gene but not in the *SLC39A8* gene. This probably happened as a stochastic event and then became fixed in the mammalian ancestral genome, because having exons 4A plus 4B in two different ZIP14 transporters must have conferred a selective advantage (i.e., greater success in fertility, reproduction, viability, or defense against the environment).

Between mouse and human, each internal exon has very similar, if not identical, lengths, and the exon-intron junctions are highly conserved (Table 1). The only differences are in multiples of three base pairs; this is commonly seen during evolution of different species, wherein an extra amino acid or two is added at the beginning or the end of an exon (in one species but not the other), but the final result is to maintain the open reading frame of the mRNA.

Since the human-rodent split ~65 million years ago, we conclude that no *SLC39* genes have been lost or gained between these two species. *Takefugu rubripes* (pufferfish) has one *SLC39* gene that shows similarly high homology to mouse (and human) *SLC39A14* and *SLC39A8*; this finding indicates that either *SLC39A14* or *SLC39A8* diverged from the other (via a gene duplication event) after the land animal-sea animal split ~425 million years ago (Fig. 1A), after which some selective advantage compelled both transporter genes to remain in the land-animal branch.

Tissue Distribution of ZIP14 versus ZIP8 mRNA. Of six tissues examined, we found C57BL/6J mouse ZIP14A mRNA levels to be twice as high in liver as in duodenum, and kidney third highest, with half that found in duodenum; ZIP14B mRNA levels were closely similar but ranked as liver > duodenum > brain > testis > kidney > lung (Fig. 3). In the only other study we could find on this topic (Liuzzi et al., 2006), two CD-1 mice were pooled, and ZIP14 mRNA by Q-PCR analysis was highest in duodenum > jejunum > liver = heart > kidney > spleen = pancreas. Thus, it appears that ZIP14 expression is highest in the liver, gastrointestinal tract, kidney, and heart. Whether these relative differences between ZIP14A and ZIP14B transcripts in different organs have any functional significance has not yet been determined.

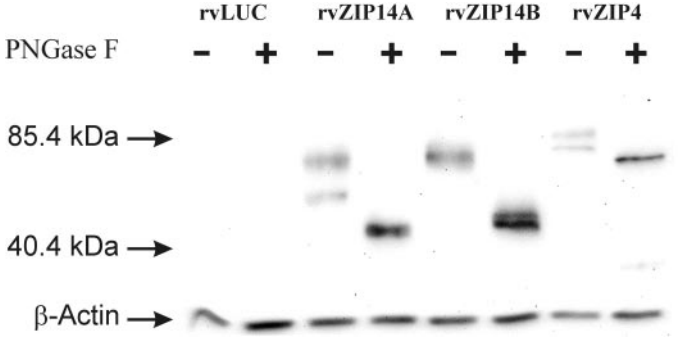

Fig. 8. Western immunoblot of proteins from control rvLUC, rvZIP14Aha, rvZIP14Bha, and rvZIP4ha—with or without PNGase F treatment. All three ZIP proteins are tagged with hemagglutinin; thus, the α-HA antibody was used. Rat β-actin protein was used to control for lane-loading. Markers (kilodaltons) are shown on the left.

We found mouse ZIP8 mRNA levels to be twice as high in lung and testis, relative to that in kidney (Fig. 3, right). Northern blot analysis of untreated C57BL/6J mice (Wang et al., 2007) agrees with the present Q-PCR data. We have also found that mouse yolk sac and placenta contain substantial levels of both ZIP14 and ZIP8 mRNA (B. Wang and D. W. Nebert, manuscript in preparation). An earlier extensive study via Northern blot (Begum et al., 2002) showed that human ZIP8 mRNA levels are most abundant in the pancreas > lung > placenta > liver = thymus ≫ spleen = testis = ovary = small intestine. Although we might conclude that human ZIP8 expression is highest in pancreas, lung, placenta, and liver, these data indicate that there might be important species differences between mouse and human in ZIP8 expression in other tissues. Expressed-sequence tags for ZIP14 and ZIP8 cDNAs are ubiquitous, however, and both can be found in more than 30 mouse and human tissues and cell types (http://www.ncbi.nlm.nih.gov).

Metal Uptake and Cell Survival. Intriguingly, Fig. 4 shows that Cd^{2+} uptake parallels cell damage, whereas Mn^{2+} uptake does not. We believe the difference between the cell toxicity profile for Cd^{2+} and Mn^{2+} is related to the ability of Cd^{2+} to bind up irreversibly the intracellular thiols (by a two-electron mechanism); Mn^{2+} lacks this electrophilic property.

ZIP14B and ZIP8 show the highest affinities for Cd^{2+} and for Mn^{2+} (Table 2). Given the tissues where these transporters are expressed at the highest levels, it is likely that when environmental Cd^{2+} (usually at very low levels) enters the body, by ingestion or inhalation, these two transporters would take it up at the interface between the environment and the organism's portal-of-entry tissues.

We attempted also to study Zn^{2+} influx but found that Zn^{2+} uptake in rvZIP14 cells, as had been found in rvZIP8 cells (He et al., 2006), was problematic. In rvZIP cells, Zn^{2+} uptake kinetics could not be quantified—as far as calculating reasonable V_{max} or K_m values. This is most probably due to the obscuring effects of too many other Zn^{2+} transporters on the surface of mammalian cells in culture. We have therefore studied Zn^{2+} transport in *X. laevis* oocytes, which are known to have negligible amounts of interfering transporters (Bossi et al., 2007) compared with any transporter cRNA being microinjected. Indeed, preliminary experiments with ZIP8-injected oocytes have determined the very low K_m values of 0.26 ± 0.09 and 0.48 + 0.08 μM for Zn^{2+} and Cd^{2+} uptake, respectively (Liu et al., 2008). We expect similar low K_m values in ZIP14 cRNA-injected oocytes.

Metal-Mediated Competitive Inhibition of Cd^{2+} Uptake. The best inhibitor of ZIP14-mediated Cd^{2+} uptake is Zn^{2+}, followed by Mn^{2+} and Cu^{2+} (Fig. 5). Consistent with this finding, ZIP8-mediated Cd^{2+} uptake is most inhibited by Zn^{2+} in *X. laevis* oocytes (Liu et al., 2008). The inhibitory data for Mn^{2+} (Fig. 5) are similar to what was found for ZIP8 in MFF cultures (He et al., 2006). Finding Cu^{2+} as a significant inhibitor of ZIP14-mediated Cd^{2+} uptake (Fig. 5) is a surprise, because Cu^{2+} did not inhibit ZIP8-mediated Cd^{2+} uptake (He et al., 2006).

We did not find Fe^{2+} to be an inhibitor of Cd^{2+} influx (Fig. 4). This observation contradicts a recent observation (Liuzzi et al., 2006) suggesting that ZIP14 mediates nontransferrin-bound Fe^{2+} into cells. Those Fe^{2+} uptake experiments were

carried out in cultured human embryonic kidney 293H cells, Sf9 insect cells, and AML12 mouse hepatocytes, whereas our experiments were carried out in MFF cultures; we do not understand why there should be this discrepancy. In the end, ZIP14-mediated Fe^{2+} uptake in the intestine or liver will need to be examined in the intact animal.

Dependence of ZIP14-Mediated Cd^{2+} Uptake on HCO_3^- Ion. As was found with ZIP8 (He et al., 2006), ZIP14-mediated Cd^{2+} uptake is dependent on extracellular HCO_3^- levels, and very low concentrations of DIDS are highly effective at blocking Cd^{2+} uptake when extracellular HCO_3^- is 171 μM (Fig. 6). These data indicate that HCO_3^- is essential for ZIP14-mediated Cd^{2+} influx.

As was found for ZIP8, both ZIP14A and ZIP14B transporters can thus be regarded as Cd^{2+}/HCO_3^- symporters. Apparently, any differences in exon 4 between these two proteins do not affect this absolute dependence on the HCO_3^- anion. It has been demonstrated recently in *X. laevis* oocytes that the $Cd^{2+}/(HCO_3^-)_2$ or $Zn^{2+}/(HCO_3^-)_2$ complex transported by ZIP8 is electroneutral and that the ZIP8 transporter is largely internalized under conditions of replete Zn^{2+}, whereas it undergoes trafficking to the cell surface under conditions of Zn^{2+} depletion (Liu et al., 2008).

Membrane Localization and Characterization of ZIP14 Transporters. We have shown that the membrane-bound ZIP14A and ZIP14B transporters are localized to the apical surface (Fig. 7) and generally glycosylated (Fig. 8). These findings are similar to what has been found with ZIP8 (Dalton et al., 2005; He et al., 2006) and ZIP4 (Dufner-Beattie et al., 2003, 2004; Liuzzi et al., 2004; Huang et al., 2006). In contrast, the ZIP5 transporter has been localized to the basolateral surface (Wang et al., 2004). ZIP14 has four potential glycosylation sites: Asn75, Asn85, Asn100, and Asn455; ZIP8 has two potential *N*-linked glycosylation sites, Asn40 and Asn88 (Fig. 2).

Concluding Remarks. The present study has shown that the mouse *Slc39a14* and *Slc39a8* genes are very similar, both with nine exons and three alternatively spliced noncoding exons 1; *Slc39a14* has the additional characteristic of two alternatively spliced exons 4. We have also shown that ZIP14A and ZIP14B transporters share many properties with ZIP8: Cd^{2+} and Mn^{2+} uptake with K_m values in the micromolar range, rendering cells sensitive to Cd^{2+} toxicity; inhibition of Cd^{2+} uptake by Mn^{2+}; HCO_3^- dependence for divalent cation uptake; localization to the apical membrane of polarized epithelial MDCK cells; and glycosylation of the transporter proteins. An observation with the ZIP14 transporter, not seen with ZIP8, is the inhibition of Cd^{2+} uptake by Zn^{2+} and Cu^{2+}; however, inhibition of ZIP8-mediated Cd^{2+} uptake by Zn^{2+} and Cu^{2+} has been demonstrated in *X. laevis* oocytes (Liu et al., 2008).

Differences in tissue-specific expression were also seen between ZIP14 and ZIP8. We found ZIP14A + ZIP14B transcript levels to be highest in the liver, duodenum, and kidney, whereas ZIP8 levels are highest in lung, testis, and kidney. It seems likely that both ZIP14 and ZIP8 play important roles in Zn^{2+} homeostasis. Their presence in cells at the interface—between the lumen and epithelial cells of the small intestine, and between inhaled air and alveolar cells of the lung—could be essential in combating Zn^{2+} loss during important critical life processes such as inflammation and immune function. Unfortunately, the location and high affinity for Cd^{2+} of the ZIP14A, ZIP14B, and ZIP8 transporters can also serve as the means for bringing unwanted environmental Cd^{2+} into these tissues.

Acknowledgments

We thank our colleagues for many fruitful discussions and careful readings of this manuscript. We especially appreciate Marian Miller for assistance with graphics and David R. Nelson for bioinformatics help with the *SLC39* gene superfamily.

References

Bannon DI, Abounader R, Lees PS, and Bressler JP (2003) Effect of DMT1 knockdown on iron, cadmium, and lead uptake in Caco-2 cells. *Am J Physiol Cell Physiol* **284:**C44–C50.

Begum NA, Kobayashi M, Moriwaki Y, Matsumoto M, Toyoshima K, and Seya T (2002) Mycobacterium bovis BCG cell wall and lipopolysaccharide induce a novel gene, *BIGM103*, encoding a 7-TM protein: identification of a new protein family having Zn-transporter and Zn-metalloprotease signatures. *Genomics* **80:**630–645.

Bergeron PM and Jumarie C (2006) Reciprocal inhibition of Cd^{2+} and Ca^{2+} uptake in human intestinal crypt cells for voltage-independent Zn-activated pathways. *Biochim Biophys Acta* **1758:**702–712.

Bergwitz C, Wendlandt T, Potter E, Glomb I, Gras K, von zur Muhlen A, and Brabant G (2000) A versatile chondrogenic rat calvaria cell line R-TTA-24 that permits tetracycline-regulated gene expression. *Histochem Cell Biol* **113:**145–150.

Bossi E, Fabbrini MS, and Ceriotti A (2007) Exogenous protein expression in Xenopus oocytes: basic procedures. *Methods Mol Biol* **375:**107–131.

Bressler JP, Olivi L, Cheong JH, Kim Y, and Bannona D (2004) Divalent metal transporter-1 in lead and cadmium transport. *Ann N Y Acad Sci* **1012:**142–152.

Cabantchik ZI and Greger R (1992) Chemical probes for anion transporters of mammalian cell membranes. *Am J Physiol* **262:**C803–C827.

Cao B, Porollo A, Adamczak R, Jarrell M, and Meller J (2006) Enhanced recognition of protein transmembrane domains with prediction-based structural profiles. *Bioinformatics* **22:**303–309.

Dalton TP, He L, Wang B, Miller ML, Jin L, Stringer KF, Chang X, Baxter CS, and Nebert DW (2005) Identification of mouse SLC39A8 as the transporter responsible for cadmium-induced toxicity in the testis. *Proc Natl Acad Sci U S A* **102:**3401–3406.

Dufner-Beattie J, Kuo YM, Gitschier J, and Andrews GK (2004) The adaptive response to dietary zinc in mice involves the differential cellular localization and zinc regulation of the zinc transporters ZIP4 and ZIP5. *J Biol Chem* **279:**49082–49090.

Dufner-Beattie J, Wang F, Kuo YM, Gitschier J, Eide D, and Andrews GK (2003) The acrodermatitis enteropathica gene ZIP4 encodes a tissue-specific, zinc-regulated zinc transporter in mice. *J Biol Chem* **278:**33474–33481.

Elisma F and Jumarie C (2001) Evidence for cadmium uptake through NRAMP2: metal speciation studies with Caco-2 cells. *Biochem Biophys Res Commun* **285:**662–668.

Fay RM and Mumtaz MM (1996) Development of a priority list of chemical mixtures occurring at 1188 hazardous waste sites, using the HAZDAT database. *Food Chem Toxicol* **34:**1163–1165.

He L, Girijashanker K, Dalton TP, Reed J, Li H, Soleimani M, and Nebert DW (2006) ZIP8, member of the solute-carrier-39 (SLC39) metal-transporter family: characterization of transporter properties. *Mol Pharmacol* **70:**171–180.

Hediger MA, Romero MF, Peng JB, Rolfs A, Takanaga H, and Bruford EA (2004) The ABCs of solute carriers: physiological, pathological and therapeutic implications of human membrane transport proteins. Introduction. *Pflugers Arch* **447:**465–468.

Hinkle PM and Osborne ME (1994) Cadmium toxicity in rat pheochromocytoma cells: studies on the mechanism of uptake. *Toxicol Appl Pharmacol* **124:**91–98.

Huang ZL, Dufner-Beattie J, and Andrews GK (2006) Expression and regulation of SLC39A family zinc transporters in the developing mouse intestine. *Dev Biol* **295:**571–579.

Järup L (2002) Cadmium overload and toxicity. *Nephrol Dial Transplant* **17 (Suppl 2):**35–39.

Järup L (2003) Hazards of heavy metal contamination. *Br Med Bull* **68:**167–182.

Järup L, Berglund M, Elinder CG, Nordberg G, and Vahter M (1998) Health effects of cadmium exposure—a review of the literature and a risk estimate. *Scand J Work Environ Health* **24 (Suppl 1):**1–51.

Jin T, Wu X, Tang Y, Nordberg M, Bernard A, Ye T, Kong Q, Lundstrom NG, and Nordberg GF (2004) Environmental epidemiological study and estimation of benchmark dose for renal dysfunction in a cadmium-polluted area in China. *Biometals* **17:**525–530.

Li HC, Szigligeti P, Worrell RT, Matthews JB, Conforti L, and Soleimani M (2005) Missense mutations in Na^+/HCO_3^- cotransporter NBC1 show abnormal trafficking in polarized kidney cells: a basis for proximal renal tubular acidosis. *Am J Physiol Renal Physiol* **289:**F61–F71.

Liu Z, Li H, Soleimani M, Girijashanker K, Reed JM, He L, Dalton TP, and Nebert DW (2008) Cd^{2+} versus Zn^{2+} uptake by the ZIP8 HCO_3^--dependent symporter: kinetics, electrogenicity and trafficking. *Biochem Biophys Res Commun* **365:**814–820.

Liuzzi JP, Aydemir F, Nam H, Knutson MD, and Cousins RJ (2006) ZIP14 (*Slc39a14*) mediates non-transferrin-bound iron uptake into cells. *Proc Natl Acad Sci U S A* **103:**13612–13617.

Liuzzi JP, Bobo JA, Lichten LA, Samuelson DA, and Cousins RJ (2004) Responsive transporter genes within the murine intestinal-pancreatic axis form a basis of zinc homeostasis. *Proc Natl Acad Sci U S A* **101:**14355–14360.

Liuzzi JP, Lichten LA, Rivera S, Blanchard RK, Aydemir TB, Knutson MD, Ganz T, and Cousins RJ (2005) Interleukin-6 regulates the zinc transporter ZIP14 in liver

and contributes to the hypozincemia of the acute-phase response. *Proc Natl Acad Sci U S A* **102:**6843–6848.
Okubo M, Yamada K, Hosoyamada M, Shibasaki T, and Endou H (2003) Cadmium transport by human NRAMP2 expressed in *Xenopus laevis* oocytes. *Toxicol Appl Pharmacol* **187:**162–167.
Olivi L and Bressler J (2000) Maitotoxin stimulates Cd influx in Madin-Darby kidney cells by activating Ca-permeable cation channels. *Cell Calcium* **27:**187–193.
Olivi L, Sisk J, and Bressler J (2001) Involvement of DMT1 in uptake of Cd in MDCK cells: role of protein kinase C. *Am J Physiol Cell Physiol* **281:**C793–C800.
Park JD, Cherrington NJ, and Klaassen CD (2002) Intestinal absorption of cadmium is associated with divalent metal transporter-1 in rats. *Toxicol Sci* **68:**288–294.
Shibuya I and Douglas WW (1992) Calcium channels in rat melanotrophs are permeable to manganese, cobalt, cadmium, and lanthanum, but not to nickel: evidence provided by fluorescence changes in FURA-2-loaded cells. *Endocrinology* **131:**1936–1941.
Tallkvist J, Bowlus CL, and Lonnerdal B (2001) DMT1 gene expression and cadmium absorption in human absorptive enterocytes. *Toxicol Lett* **122:**171–177.
Waalkes MP (2003) Cadmium carcinogenesis. *Mutat Res* **533:**107–120.
Waisberg M, Joseph P, Hale B, and Beyersmann D (2003) Molecular and cellular mechanisms of cadmium carcinogenesis. *Toxicology* **192:**95–117.
Wang B, Schneider SN, Dragin N, Girijashanker K, Dalton TP, He L, Miller ML, Stringer KF, Soleimani M, Richardson DD, et al. (2007) Enhanced cadmium-induced testicular necrosis and renal proximal tubule damage caused by gene-dose increase in a *Slc39a8*-transgenic mouse line. *Am J Physiol Cell Physiol* **292:**C1523–C1535.
Wang F, Kim BE, Dufner-Beattie J, Petris MJ, Andrews G, and Eide DJ (2004) Acrodermatitis enteropathica mutations affect transport activity, localization and zinc-responsive trafficking of the mouse ZIP4 zinc transporter. *Hum Mol Genet* **13:**563–571.
Zalups RK and Ahmad S (2003) Molecular handling of cadmium in transporting epithelia. *Toxicol Appl Pharmacol* **186:**163–188.

Address correspondence to: Daniel W. Nebert, Department of Environmental Health, University of Cincinnati Medical Center, P.O. Box 670056, Cincinnati, OH 45267-0056. E-mail dan.nebert@uc.edu